Influence of operating conditions on wetting and wettability in membrane distillation using Detection of Dissolved Tracer Intrusion (DDTI)

Paul Jacob, Tianyi Zhang, Stéphanie Laborie, Corinne Cabassud

Influence of operating conditions on wetting and wettability in membrane distillation using Detection of Dissolved Tracer Intrusion (DDTI)

Paul Jacob[a], Tianyi Zhang[a], Stephanie Laborie[a] and Corinne Cabassud[a]

[a] LISBP, Université de Toulouse, CNRS, INRA, INSA, Toulouse, France

Corresponding author: corinne.cabassud@insa-toulouse.fr

Abstract

This study aimed to evaluate the effects of operating parameters (temperature (T_f), Reynolds number (Re), and salinity) on wettability (contact angle, liquid entry pressure and surface free energy) and wetting indicators evaluated with the recently developed Detection of Dissolved Tracer Intrusion (DDTI) method in Vacuum Membrane Distillation (VMD) for desalination. A 0.22 µm PVDF membrane was subjected to VMD considering a large NaCl feed salinity (22 to 310 g/L). In a first step, the effects and interactions of the operating parameters on the totally wetted surface ratio (ω_s) was studied using Box Behnken design of experiments. It was shown that for salt concentrations below 166 g/L the ω_s is low and is poorly affected by Re and T_f, whereas for a salt concentration of 310 g/L the influence of T_f and Re becomes sensitive, and high T_f and high Re are required to avoid wetting. In a second step, the effect of salinity was evaluated as a proportion of the liquid intrusion. Here it appears that the range of salinity influences the wetting mechanisms, with an evidence of total wetting only for hypersaline concentrations (higher than 200 g/L).

Keywords

Membrane distillation; Salinity; Wetting influencing parameters; Wetting detection; Wettability indicators

Highlights

1. For low to high salinities (<200 g/L) surface wetting occurs but total wetting is not detectable
2. For hypersaline solutions (>200 g/L) both surface and total wetting occur
3. For hypersaline solutions, higher Re and T allow to reduce the risk of total wetting
4. Total pore wetting occurrences for hypersaline solutions are more frequent
5. CA and SFE reveal much more information on wettability than LEP

Graphical abstract

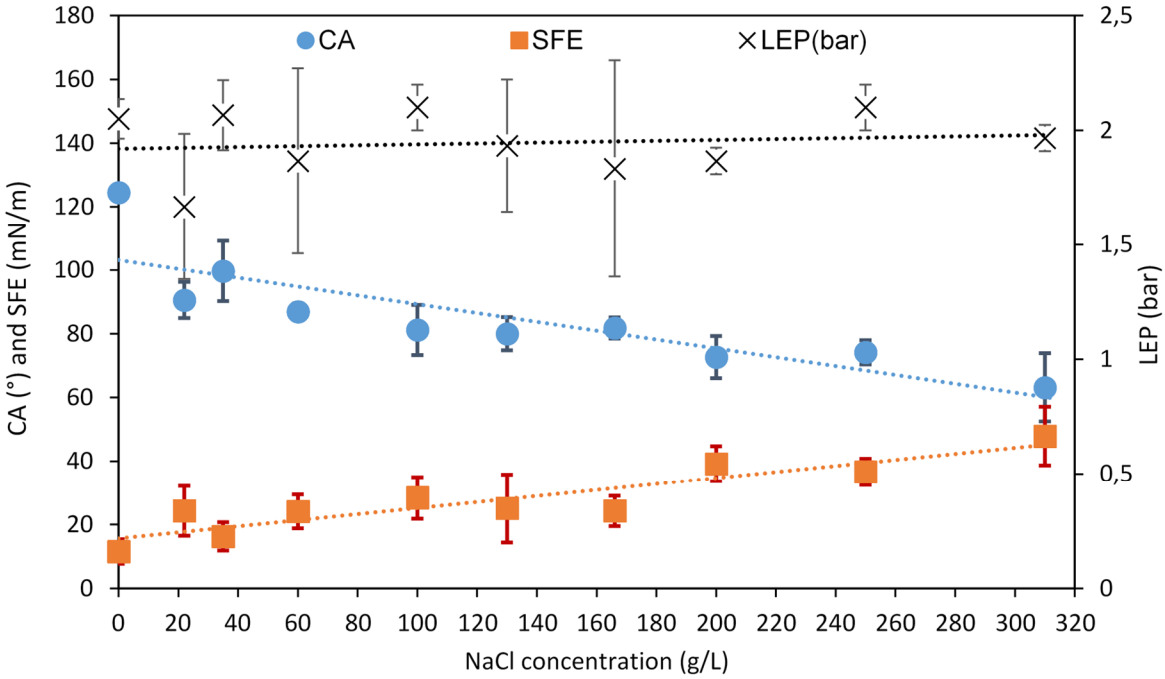

1. Introduction

The challenges arising due to water security with population growth and climate change has led to United Nations recognizing the importance of Goal 6 of its 2030 Agenda for Sustainable Development Goals (SDG) to ensure the availability and sustainable management of water. Over 2 billion people lack safe drinking water with water demands being expected to increase by nearly one-third by 2050. Better technological and managerial solutions are needed to offset these problems and tackle them at its core. Thereby the current focus is towards desalination of the oceans. Analysts forecast the global market on desalination to have an annual growth rate of 8.6 % during the period 2018-2022 [1]. Membrane distillation (MD) can treat hypersaline solutions with substantially greater salinities than reverse osmosis with similar footprint [2] and thus RO and MD can be coupled [3]. MD can also be associated with renewable energies, like solar energy [4].These major differential advantages arouse a growing interest for the industrial development of this technology.

However, membrane wetting is a primary barrier for MD's scale up as an industrial process [5,6] even if the risks of wetting occurrence and of the related process dysfunction are not well understood and qualified. To further assist this innovative technology for full scale engineering applications, one of the factual hitches it faces is for the pores to remain dry amid operation to safeguard a decent permeate quality [7]. Historically, wetting in membrane distillation is principally evaluated using liquid entry pressure (LEP) by experimentally evaluating the wetting pressure of a given hydrophobic membrane. With respect to the predicting wetting, several modelling efforts have been made but primarily focusing towards improving the LEP models. The standard model for capillarity were firstly adapted and used for predicting LEP by adjusting the Young-Laplace (YL) equation modified by others [8,9]. Finally a geometrical factor was added to adjust for the pore structure resulting in the commonly accepted Franken model [10]. Since then further efforts have been made by several authors for example Kim and Harriott [11] with the most recent being a CFD approach to LEP predication [12]. There are some newer studies that have moved away from LEP modelling and started to focus on pore wetting itself [13].

From an experimental stance, wetting in membrane distillation is commonly evaluated by using LEP, surface free energy (SFE) and contact angle (CA) measurements. However, these

parameters are only indicating the potentiality of the membrane to be wetted i.e. membrane wettability, as these indicators have not proven to be precisely predictive. So, confusion exists in the literature between wetting and wettability. With the accelerated interest to apprehend wetting, researchers have also developed both ex-situ [14] and in-situ [15] detection tools to evaluate and understand this phenomenon. The most common technique for in-situ wetting detection is by measuring the conductivity of the permeate. Using this tool, the only information that can be attained is that some pores on the membrane surface are totally wet during operation and filtration is occurring instead of phase change of the feed solution. However, in this paper, we focus on a utilizing a recently developed Detection of Dissolved Tracer Intrusion (DDTI) method which visualizes and classifies wetting at the pore scale using microscopic and spectroscopic techniques [14].

At present, most studies are ambiguous on the effects of operating conditions and feed characteristics and their interactions on wetting. However, some information can be distinguished that really relies on wetting [16–18] but are principally focused on DCMD configuration. For example, the effects of varying flowrates and temperatures at constant salinity in the DCMD process were illustrated by using the rise in conductivity (wetting rate, $\mu S\ min^{-1}$) employing mass balance[19]. It was concluded that at the higher feed temperatures (50 and 60°C) the time to wet the membrane could be possibly delayed, whereas, the effect of flow rates on wetting was considered marginal. On the effect of process parameters on membrane material itself, Eykens et. al [20] studying DCMD configuration presented that at higher salinities a thicker membranes would be much suitable but these conclusions where targeted towards energy efficiency as wetting was not reported. Other observations made using SEM, pore size distribution (PSD) to study the microstructure evolution of membrane pores at different temperatures concluded that exposure to high temperature (40 – 70 °C) could induce wetting [17]. Only a few available studies are directly addressing or assessing the effects of operating parameters [16,18,19] on wetting. Some papers did consider the composition of feed solution [21,22], but for oil emulsions. Thus, the effects of process parameters on wetting are unsettled, and a more systematic approach still needs to be developed as there is uncertainty in the interactive effect of process parameters to induce wetting.

Therefore, the overall objective of this study is on the possible application of MD for desalination by analyzing the influence of operating parameters and feed salinity on wetting mechanisms in vacuum membrane distillation by:

- An ex-situ characterization of wetting using the DDTI method that has been previously developed in our group [14], allowing to obtain two wetting indicators, i.e. totally wetted surface ratio (ω_s) and pore wetting ratio (ω_p). These indicators aid in visualizing wetting mechanism by the salt traces it has left inside the membrane during operation.
- Determination of wettability by classical indicators (CA, SFE, and LEP)

The first part of this study aimed to qualify the effects and interactions of temperature, Reynolds number, and salinity on total wetting using the first indicator in DDTI method (totally wetted surface ratio (ω_s)) and on wettability. The experimental strategy was based on Design of experiments (DoE). Whereas the second part of this paper aims at studying the impact of feed salinity on the location of the liquid/vapor (L/V) interface inside the membrane pores to characterize partial pore wetting using the second indicator (pore wetting ratio (ω_p)). A wide range of salt concentrations (NaCl) were considered (22 to 310 g/L).

2. Material and methods

This section presents, the detailed description, and motivation of the two strategies used for understanding wetting influences of operating parameters, the membrane and its characterization, experimental setup, and finally wetting detection tools. Overall the effects of three process parameters on wetting were studied: feed temperature (T_f), Reynolds number (Re), and salinity (C_f) in vacuum membrane distillation (VMD). **Figure 1** illustrates the overall methodology. After the initial membrane characterization, the overall study was architectured in two independent parts where wetting was evaluated based on the two developed tools and compared with wettability indicators.

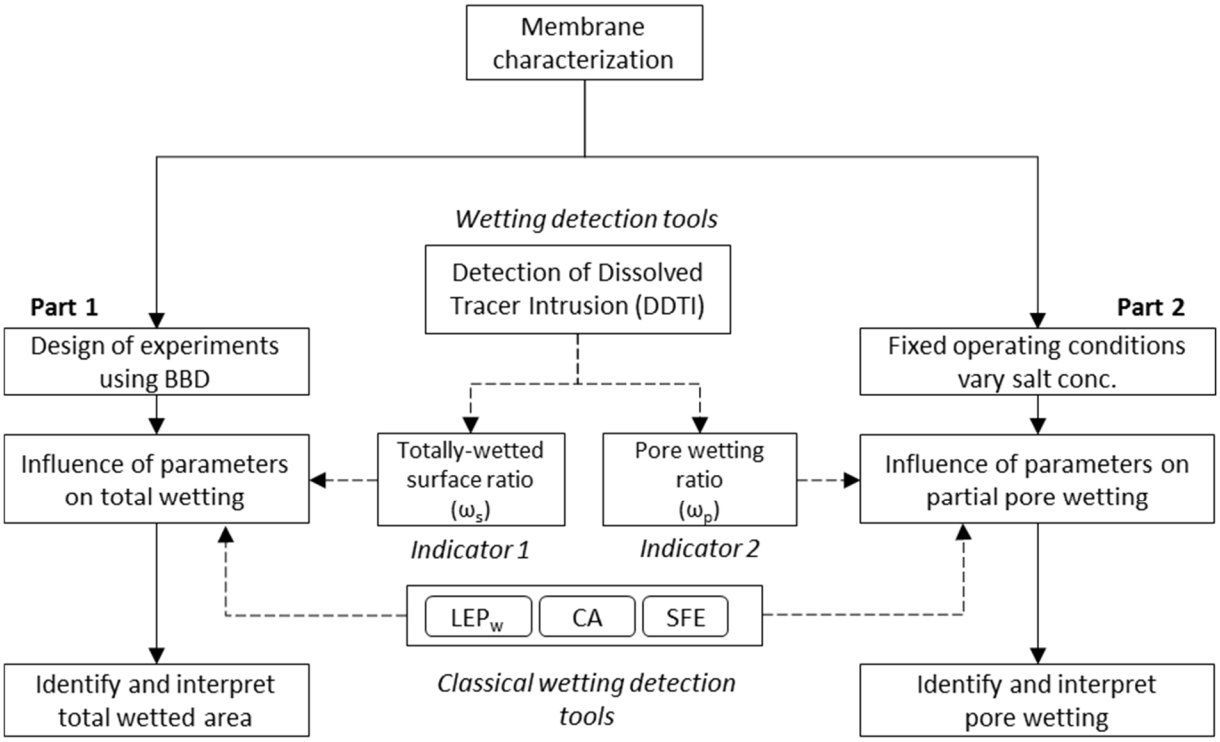

Figure 1: Overall methodology to evaluate the effects of MD parameters on wetting

2.1 Part 1: Influence of operating parameters on total wetting

Box-Behnken design (BBD), a sub-classification matrix of response surface methodology (RSM) [23] was used to study total wetting. BBD are three-level incomplete factorial designs based on second-order (partially or fully rotatable) designs. BBD is principally used for screen and select favorable factors with big ranges based on the generated experiments. The required number of experiments (N) to develop a statistically valid BBD is defined in Eq. 1.

$$N = 2k(k - 1) + C_0 \quad \text{Eq. 1}$$

Where, k is number of factors and C_0 is the number of central points.

Application of RSM models for membrane characterization and process optimization is common in membrane distillation. This methodology has been applied to configurations like DCMD [19,24,25], SGMD [26], AGMD [27] for both membrane characterization and process optimization. The DoE was prepared using Design Expert (V10) considering the three selected operating factors. **Table 1** presents the low and high values of each factor. Feed temperatures

(T_f) varied between 35 – 50 °C, whereas the Reynolds number (Re) between 382 – 4000 and the salinity (C_f) from 22 to 310 g/L of NaCl respectively. 17 experimental runs were generated using BBD, where the design points were randomized. The assigned values for the temperature (T_f) were discretized, whereas continuous values assigned for flow rate (Re) and salt concentration (C_f). Some repeat experimental runs (Run 2, 3, 6, 10 and 16) were inbuilt to ensure statistical validity.

Table 1: Factors with their minimal and maximal level used for Box-Behnken design

Factor	Name	Units	Min.	Max	Mean	S.D.
A	Temperature (T_f)	°C	35	50	42.5	5.303
B	Reynolds number (Re)	-	382	4000	2191	1279.16
C	Salinity (C_f)	g/L	22	310	166	101.82

The vacuum pressure and the total permeate volume produced for each experiment were kept constant at 6 kPa and 225 g of permeate respectively, regardless of the operating conditions. Only after the operating factors reached their desired values, experiments commenced. Experimental runs took between 4 hours to 3 days depending on the operating conditions. Each experimental run had five responses (R1-R5): R1: Flux ($kg.m^{-2}.h^{-1}$), R2: CA (°), R3: SFE (mN/m), (CA and SFE measured at 8 locations), R4: LEP (bar) (at 3 locations), and R5: ω_s (9 locations). All response data presented in section 3.1 are average values.

Analysis of variance (ANOVA) tests were performed on R1-R5 using reduced quadratic model with partial sum of squares - Type III. For each response, necessary data analysis and transformation were performed to generate statistically valid models. For the fitting model, F-value tests were conducted to compare the source's mean square to the residual mean square to determine the model's significance. Finally, the model equations were established and reported to understand the interactions within the designed space. Additionally, a comparison between experimental and model predicted data were performed to ensure the model validity.

2.2. Part 2: Influence of operating parameters on partial pore wetting

The effect of only varying salinity (C_f) while fixing temperature and vacuum pressure commonly used in VMD was studied. Here the feed salinity was varied from 22 - 310 g/L NaCl (cf. **2.4**) while the other operating conditions were fixed (T_f: 42.5 ± 0.19°C, Re 2191 and vacuum pressure 6 ± 0.011 kPa). For each experimental condition 225 g of water (a constant volume) was collected as permeate. Depending on the salt concentration the experiment lasted between 9.6 h to 24 h.

2.3. Membrane properties

A PVDF microporous membrane (Durapore, GVHP29325) was used throughout the study, as this membrane has been widely considered for numerous MD configurations [3,28,29]. Its characteristics are presented in Table 2:

Table 2: Properties of the virgin reference membrane (Durapore, GVHP29325 by Millipore)

Pore size (µm)	Thickness (µm)	Porosity (%)	Contact angle (°)	SFE (mN/m)	LEP_w (kPa)	K_M ($mol^{1/2}.m^{-1}Kg^{-1/2}$)
0.28	117.7	75	124	11.5	204	$3.59\ 10^{-6}$

The membrane's Knudsen permeability coefficient (K_M) and water liquid entry pressure (LEP_w) were experimentally determined using techniques previously described elsewhere [14].

2.4. Saline solutions preparation

Saline solutions were prepared using NaCl (> 99% pure, Fisher Scientific, France) diluted in ultra-pure water. The range of salt concentrations (22- 310 g/L) was chosen to cover concentrations observed from brackish waters [30] to reverse osmosis concentrates, as there is an increasing interest in using MD to treat RO brines, and to membrane distillation crystallizers [18]. For each experimental run, a 4L solution was prepared and the saline solution was pre-heated before each experimental run.

2.5. Vacuum membrane distillation setup and operating conditions

The prepared saline solution was maintained at the desired temperature in the feed tank using jacketed heat exchanger on the VMD setup (**Figure 2**). K-type sensors (accuracy ±1.6 %) were used for measuring temperature before the module feed inlet (T1) and at the module retentate outlet (T2). The feed velocity on the membrane surface (Area = 4.16 x 10^{-3} m^2) was controlled using a flow meter (Krohne, 0-250 L/h) by adjusting a magnetic pump in a closed loop. The Reynolds number (Re) was calculated using Eq. 2.

$$\mathrm{Re} = \frac{\rho . \mathrm{D_h} . \mathrm{v}}{\mu} \qquad \text{Eq. 2}$$

Where, ρ, D_h , v and μ are the fluid density (kg/m^3), effective diameter (m), average fluid velocity inside the feed compartment (m/s) and dynamic fluid viscosity (kg/m.s) respectively. The effective diameter was calculated considering internal flow in a rectangular chamber by employing the following equation Eq. 3:

$$D_h = \frac{(2\mathrm{h} * \mathrm{b})}{(\mathrm{h} + \mathrm{b})} \qquad \text{Eq. 3}$$

where

h = height of the membrane feed compartment (m)

b = breath of the membrane feed compartment (m)

The effective diameter used in the study with the membrane cell dimensions were 9.89 x 10-4 m.

The values for these constants (ρ, v, and μ) at different operating temperatures(T_f) were taken from standard reference [31].

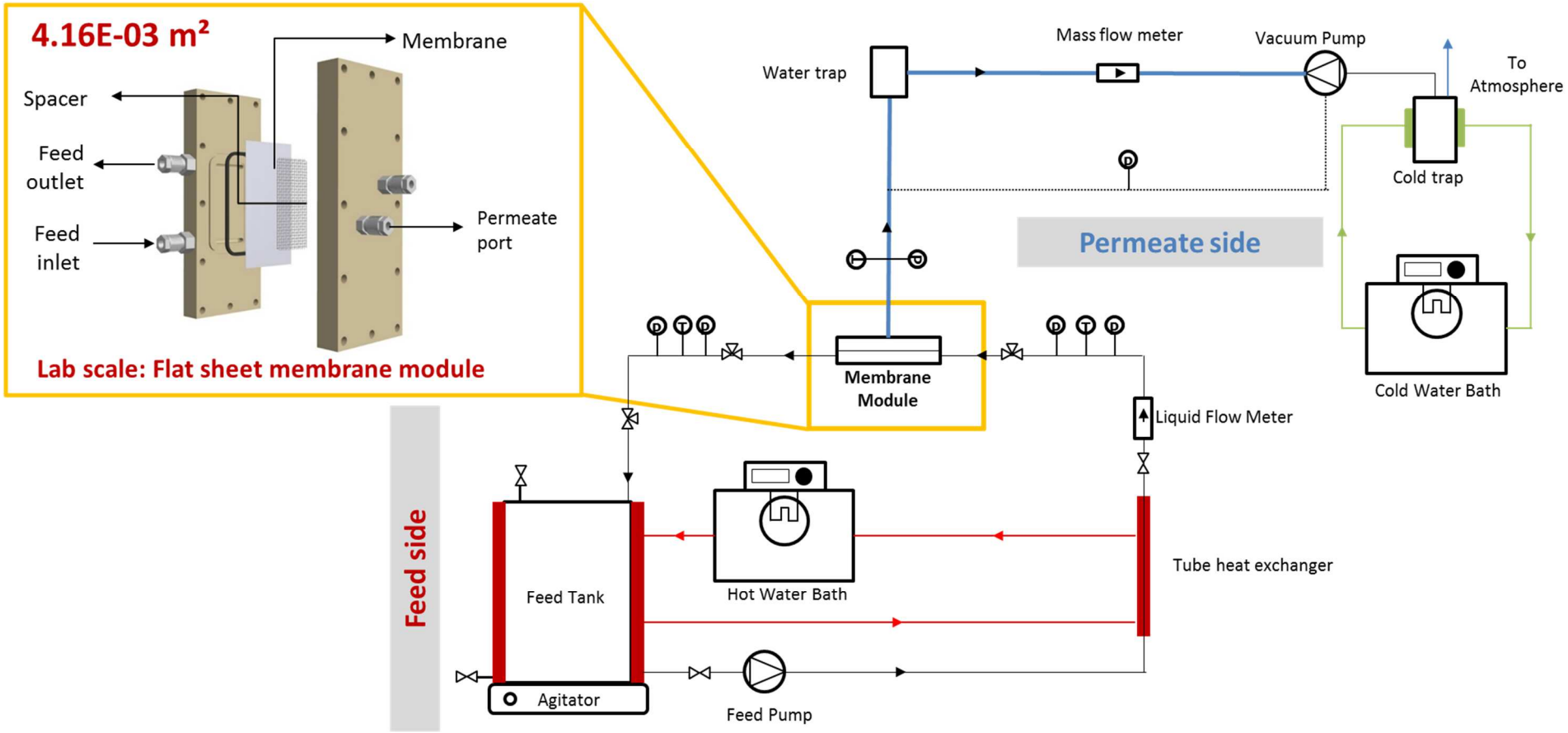

Figure 2: Schematic of vacuum membrane distillation setup and the membrane cell (to be viewed in color)

The membrane was supported by a spacer on the vacuum side only. Temperatures, pressures, conductivities were measured at all inlets and outlet of the membrane module. All sensors logged data onto a computer for the total duration of each experiment. The VMD setup was insulated to prevent heat loss. A detailed description of the experimental setup can be found elsewhere [14]. The permeate flux was calculated using a mass flow meter using Eq. 4.

$$J = \frac{\text{vapor flux}}{1000 \times A} \qquad \text{Eq. 4}$$

Where J is flux ($kg.m^{-2}.h^{-1}$), vapor flux (g/h) and A (active membrane area, m^2)

2.6. Wetting detection tools

The two wetting indicators obtained with the DDTI method were used together with wettability indicators like CA, SFE, and LEP_w. Following sub-section introduces a brief description of wetting and wettability detection tools. These tools were used together for understanding the influence of the operating parameters towards wetting in membrane distillation.

2.6.1. The Detection of Dissolved Tracer Intrusion (DDTI) method

The method was developed and validated in a previous study [14]. It exploits the fact that during MD operation if wetting occurs, dissolved feed solutes (tracers) progressively penetrate the cross-section of the membrane. These tracers can be detected by coupling electron microscopic and spectroscopic techniques. A Scanning electron microscope (SEM) (JEOL, JSM-6400) coupled with X-ray energy-dispersive spectrometry (EDX) (Bruker, XFlash 6130) were used for obtaining SEM and elemental spectroscopy data. The high tension of the SEM was 20 KeV and the resolution of the EDX detector was 125 eV with a detector surface area of 30 mm^2.The tracer intrusion was measured by Cl^- intensities on and inside the membrane surface and cross-section using the developed indicators respectively.

The two indicators assess localized wetting distinctively in the following manner:

- Totally-wetted surface ratio (ω_s), quantifies wetting by determining the ratio of the permeate surface covered by the tracer compared to the observable membrane length.
- Whereas, pore wetting ratio (ω_p), quantifies the ratio of the tracer intrusion inside the membrane cross-section as compared to the total observable membrane cross-section.

For pore wetting ratio (ω_p), the penetration depth of the tracer from the feed to the permeate side of the membrane cross-section was further classified into different wetting mechanisms and were reported based on the % penetration depth:

1. No wetting is reported if the tracer intensity peaks at 0 - 1 % of the membrane cross-section (on the feed side of the membrane surface)
2. Surface wetting is reported if the intensity peaks at 1.1-10 % inside the membrane cross-section
3. Partial wetting is reported if the intensity peaks at 10.1-90 % inside the membrane cross-section
4. And finally, total wetting is reported if there are tracers observed at the membrane cross-section greater than 90%, that is to say the highest tracer intensities were located near the permeate side of the membrane surface.

As detailed description/definitions, criteria's and governing equations of each indicator have been presented previously [14], therefore, only the sampling locations and data treatment for each wetting indicator are presented below.

2.6.1.1. Totally-wetted surface ratio (ω_s)

This indicator was utilized in the evaluating wetting at pore scale in the first part of the study (**cf. 3.1**). After experimentation the feed side of the membrane surface was cleaned in-situ using D.I. water to remove the salt traces before sample collection. With respect to the sampling locations, each membrane was assessed at 9 locations; 3 samples were taken near the feed inlet

(A1-A3), 3 on the membrane surface (B1-B3) and 3 at the feed outlet (C1-C3) with an observed cross-section of about 258 µm. After totally-wetted surface ratio analysis, the values were averaged for the nine sampling locations and were used for further analysis for the BBD.

2.6.1.2. Pore wetting ratio (ω_p)

The results of this indicator were used in the second part of the study where no in-situ cleaning was conducted on the membrane surface before wetting analysis were done and the results are presented (cf. **3.2**). For each membrane studied, the samples were collected at 10 locations. Two samples were collected near the feed inlet (A1 – 2), 6 on the membrane surface (B1 – D2) and 3 at the feed outlet (E1 – E2) with an observed cross-section of about 258 x 117 µm. No cleaning of the membrane surface was done before using this indicator. After sample analysis, data treatment was performed for further analysis and interpretation.

Detailed on description of the sampling locations used for both indicators can be found elsewhere [14].

2.6.2. Classical wettability tools (LEP, CA and SFE)

Wettability tools were used on both virgin and post experimentation membrane surfaces to evaluate the changes caused of the operating conditions on the membrane's intrinsic properties.

LEP_w measurements were conducted to evaluate the effects on "wetting pressure." LEP_w of each membrane was assessed at 3 locations (feed inlet, membrane surface, feed outlet) and an averaged value and standard deviation were reported. Standard protocols of LEP_w measurements were used [14].

Whereas, CA and SFE analyses were performed on the membrane surface utilizing Drop Shape Analyzer (DSA25, Kruss) using standard surface science protocols [32,33] and details can be found elsewhere [14]. On the active membrane surface (feed side) 6-8 CA/SFE samples were collected and averaged results and standard deviation reported.

2.6.3. Conductivity

Additionally, conductivities were measured both in the feed and in a condensate flask on the permeate side (see **Figure 2**, C1 & C2) using calibrated conductivity probes (CONDUCELL 4UHF ARC PG-120, Hamilton).

3. Results and discussions

3.1 Part 1: Potential influence of operating parameters on total wetting

Table 3 presents the results obtained in part 1 of this study. Overall it can be noted from **Table 3**, that under respective operation conditions the flux varied between about 0 to 11.5 $kg.m^{-2}.h^{-1}$, the contact angle varied between 67.6 – 118.9°, the SFE ranged between 13.9-50.1, LEP_w varied between 120-205 kPa and finally the totally wetted surface (ω_s) was between 0 (No wetting) to 78.3 % (total wetting observed in every sample but to a varying degree).

While comparing wettability indicators with the one of the virgin membrane (CA_{ref} 124°, SFE_{ref} 11.5 mN/m and LEP_{ref} 2.04 bar) it can be noted that the operating conditions influenced these membrane properties to a varying degree. At 50°C regardless of the C_f and Re, the CA was 113.9±1.9° which was close to CA_{ref}. It is clear that for all other runs CA was lower than to CA_{ref}, and that SFE was always higher than SFE_{ref} which means that operation makes the membrane more hydrophilic. LEP was very close to LEP_{ref} for 4 runs but lower for all the others. This suggests that wettability was affected during these runs. As for wetted surface analysis, in most studied cases wetting was not found for other runs than for the ones at C_f 166-310 g/L, were wetting observations were persistent but to varying degrees (9 – 78%).

In **Table 3** it can be seen that at the lowest saline concentrations (C_f 22g/L), ω_s was in its limit of detection, which means that total wetting was not observed, even by varying Re and T_f. In the replication runs (runs 2, 3, 6 , 10 and 16, all at T_f 42.5, Re 2191, C_f =166 g/L), the dispersion for flux was 4.3 ± 0.5 $kg.m^{-2}.h^{-1}$, showing quite a good repeatability whereas there were significant

variations in CA, SFE were respectively 95.6 ± 18.1 °, 30.7 ± 14.3 mN/m and a slight variation in LEP 1.8 ± 0.2 bar. During these replicates ω_s was 0% for 3 runs and reached 10 % for one run.

Table 3: Influences of T_f, Re and C_f on flux, wettability indicators (CA, SFE, and LEP_w) and totally wetted surface indicator (ω_s)

Trial	Factor			Response				
	Temperature	Flow regime	Salinity	1	2	3	4	5
	T_f (°C)	Re (-)	C_f (g/L)	Flux ($kg.m^{-2}.h^{-1}$)	CA (°)	SFE (mN/m)	LEP_w (bar)	ω_s(%)
1	42.5	4000	22	6.3	116.4	13.9	2.00	0.0
2	42.5	2191	166	3.5	104.2	22.8	1.95	0.0
3	42.5	2191	166	4.3	67.6	41.7	1.40	10.0
4	35	2191	310	0.02	82.5	38.1	1.73	78.0
5	35	2191	22	1.2	107.9	14.6	1.70	0.0
6	42.5	2191	166	4.6	112.0	19.9	1.97	0.0
7	50	382	166	6.9	116.3	19.7	1.57	11.0
8	42.5	4000	310	1.4	103.5	34.6	1.77	9.0
9	42.5	382	310	1.4	92.7	29.7	1.73	68.0
10	42.5	2191	166	4.6	87.6	50.1	1.63	0.0
11	50	2191	310	2.8	114.3	18.8	1.50	32.0
12	50	2191	22	11.5	113.3	23.3	2.05	0.0
13	42.5	382	22	3.8	118.9	16.1	1.43	0.0
14	35	382	166	0.4	90.6	22.2	1.20	5.0
15	50	4000	166	10.1	111.7	25.3	1.53	0.0
16	42.5	2191	166	4.5	106.4	18.9	1.80	1.0
17	35	4000	166	1.1	74.8	40.1	1.60	24.0
Min				0.02	67.6	13.85	1.2	0
Max				11.47	118.9	50.1	2.05	78
Mean± S.D.				4.0± 3.1	101.2±15.2	26.5± 10.4	1.7± 0.2	14.0± 23.4

It appears that the more repeatable responses are the ones that are measured at a global scale (or at the scale of the membrane). For example, results from LEP_w are more consistent when

measured at the scale of the whole membrane area and a higher dispersion is observed for the more local indicators (For example ω_s), which are based on membrane sampling at very local scales. Thus, the dispersion can be attributed to membrane heterogeneity. This is indicative that membrane wetting is a localized phenomenon and can vary over the membrane surface depending on membrane morphology. In the following section, this question will be studied in detail (cf. **3.2)**.

Founded on the factors and responses shown in **Table 3**, empirical equations were generated to describe ω_s **(**Eq. 5**)** and wettability indicators (CA(Eq. 6), SFE (Eq. 7) and LEP) as functions of input process parameters (T_f, Re, C_f). These equations can be valid only for the operating conditions presented here, while the VMD system was operated under constant volume mode (225 g) using the presented membrane cell geometry (Figure 2) and membrane utilized.

3.1.1 Relationship between the totally-wetted surface ratio (ω_s) and operating parameters

Considering ω_s, a natural log transformation $(y' = \ln(y + k))$ was required to fit the model with a constant (k) of 0.078. It shows that ω_s principally depends on salinity (C_f) and to a lesser extent to temperature (T_f) and Reynolds number (Re). The resulting model equation is presented in Eq.5.

$$\ln(\omega_s + 0.08) = -9.33 + (0.16T_f) + (4.67 \times 10^{-3}Re) + (0.021C_f) - (1.18 \times 10^{-4}T_fRe) \quad \text{Eq. 5}$$

To understand the generated model's accuracy, the values computed with Eq. 5 were plotted against the experimental values in **Figure 3**. For ω_s, the computed and the experimental data are in good agreement for lower values, but computed values are higher than the experimental one at higher values corresponding to totally wetted surface. So, the Eq. 5 is over-estimating ω_s when wetting becomes severe (cases of run 4 and 9, both corresponding to a salt concentration of 310 g/L).

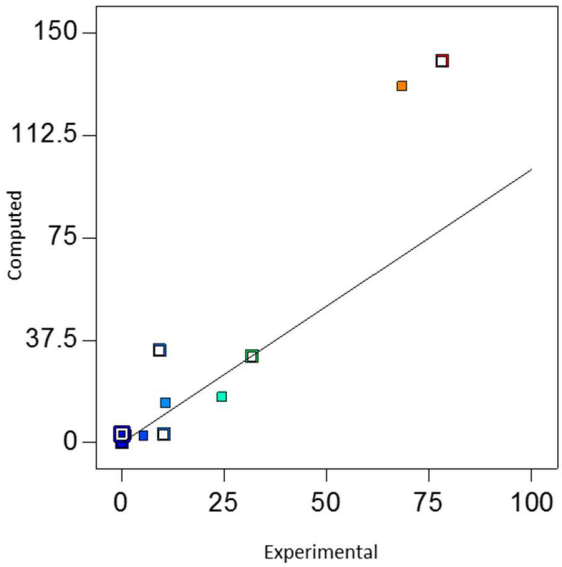

Figure 3: Computed value vs experimental data for the totally wetted surface ratio ω_s

These observed variations in computed data might be due to the limitation of BBD itself or to the fact that some parameters that may be influent have not been considered initially in our experimental strategy. Zolgharnein et al. [34], emphasized that BBD is a spherical design fitted to a cubical design not utilizing the vertices or edges of the design space. Therefore, the extreme combinations of factors (operating conditions) are not concealed in this approach and consequently, the model has greater variability at the extremities of the design space. Thus, it is safe to point out that Eq. 5 is only valid under the range of studied operating conditions, and as said before for moderate values of ωs. Interpretation based on extreme operating conditions and saline concentrations should be dealt with considerable reservations. However, the model can be used to visualize the possible tendencies in the parameter's interactions.

Using Eq. 5, ω_s was computed for saline concentrations of 22 (a), 166 (b) and 310 g/L (c) and **Figure 4** introduces the interactive effects of temperature and Reynolds number on ω_s. The x-axis presents the temperature (T_f) in the range of 35 - 50°C and the y-axis presents the Reynolds number (Re) from 382 to 4000 respectively. The lines introduced on each graph are the iso-ω_s lines and the colors are blue when ω_s is close to 0 (no wettability) and red when ω_s approaches 100%.

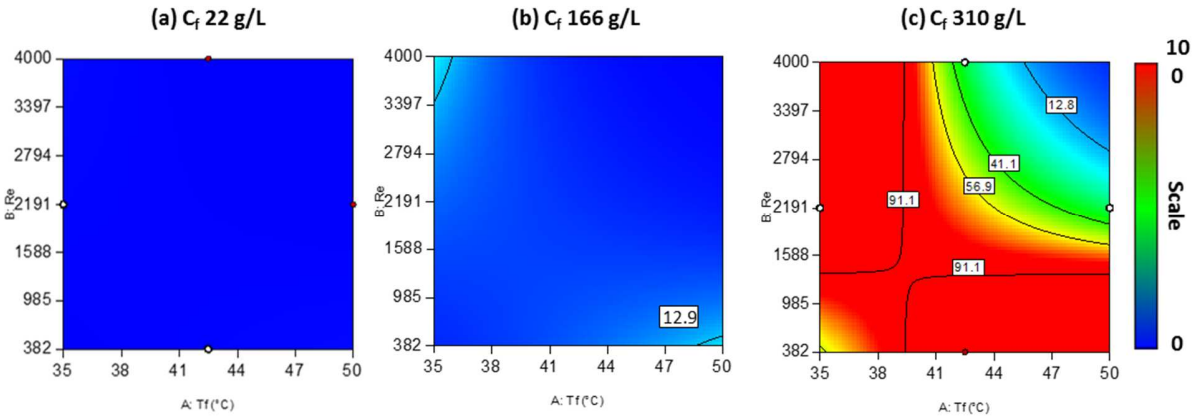

Figure 4: Computed values of totally-wetted surface ratio (ω_s) at NaCl concentrations of (a) 22 g/L (b) 166 g/L and (c) 310 g/L

As represented in **Figure 4** (a) low values of ωs, attesting non-occurrence of total wetting (low values of ωs), are observed for the lowest saline concentrations (C_f 22g/L), in all the range of T_f and Re values. As the salinity (C_f) increases to 166 g/L NaCl, (Figure 4.4 (b)), ω_s is quite low in all the experimental area and a slight increase is observed at the two extremities i.e. with the combination of highest Re (4000) and lowest temperature (35°C) and lowest Re (382) at high T_f (50°C), where computed value of ω_s was 13 % (to be compared to 24 and 11% for the corresponding experimental runs, runs 17 and 7). At the highest saline concentration, the model predicts that total wetting could become significant in a large area of the experimental domain and mainly for the lower temperatures (T_f 35 – 42.5°C). Both Re and T are influencing wetting. Depending on these parameters, wetting could be low (about 13 %) or high (91 %) if temperature or Re are low. This might be explained by the fact that at this high concentration and for low Re and low temperature, the local salt concentration at the membrane surface might be close to saturation and crystallization at the membrane surface could be a kind of inducer of pore wetting.

In conclusion, for concentrations of 22 to 166 g/L total membrane wetting is low and is poorly affected by T_f and Re. Whereas for very high concentrations of 310 g/L, the influence of T_f and Re becomes sensitive and the choice of these values is determinant to avoid wetting. Both high

temperature and high Re values are required in the process otherwise totally-wetted surface ratio can become significant.

As previously stated, factors like temperature and Reynolds number had a lower influence than salinity on wetting in this study. Normal operating conditions ($\mathrm{T_f}$ $(35-50°\mathrm{C}), \mathrm{Re}(382-4000)$) within this range do not affect wetting greatly for the current operation mode and membrane. However, if data obtained from flux, CA and SFE responses are considered, it can be concluded that $\mathrm{T_f}$ at $35°\mathrm{C}$ would not be a suitable operating condition (under any Re and C_f) for membrane distillation with a vacuum pressure of 6 kPa in this PVDF membrane. As the feed's partial pressure and the applied vacuum determines the driving force in VMD, therefore at lower temperatures, the driving force is reduced resulting in low fluxes. Additionally, as the process progresses the mass transfer (water vapor) results in an increase in feed salinity, resulting in further reduction of the driving force. This eventually results in heightened changes of nucleation sites on the membrane surface thereby increasing wetting occurrences.

In the narrow feed channel, an increase in the Re upsurges the hydrostatic pressure experienced by the membrane surface. As a result, some of the biggest pores on the feed side of the membrane get compromised therefore ensuing in pore wetting. This is due to the local hydraulic pressure generated by the fluid flow on the membrane surface exceeding the membranes intrinsic liquid entry pressure (LEP_w). Similarly Gryta [16] reported that the hydrodynamic conditions influenced total wetting in some membrane pores by observing a rise in conductivity in the permeate.

3.1.2 Relationship between the wettability indicators and operating parameters

Regarding contact angle (CA), based on the experimental run and after ANOVA tests, no transformation was required to fit the experimental data for establishing a relationship between CA and the operating parameters. Only two operating parameters, T_f and C_f are required to obtain CA, as presented in Eq. 6.

$$\mathrm{CA} = 39.75 + 1.66\mathrm{T_f} - 0.055\mathrm{C_f} \qquad \text{Eq. 6}$$

For SFE, an inverse transformation ($y' = \left({}^{1}/_{y+1}\right)$ was required to fit the model with constant (k) of -0.81. After ANOVA tests, it was found that the interactions between operating parameters and SFE energy can be described by Eq. 7.

$$\frac{1}{(\mathrm{SFE} - 0.81)} = 0.14 - (1.81 \times 10^{-3}\mathrm{T_f}) - (6.5810^{-4} \times \mathrm{C_f}) + (1.31 \times 10^{-5}\mathrm{T_f C_f}) \quad \text{Eq. 7}$$

These equations integer the fact that SFE does not depend on Re but shows a dependency on temperature($\mathrm{T_f}$) and salt concentration ($\mathrm{C_f}$).

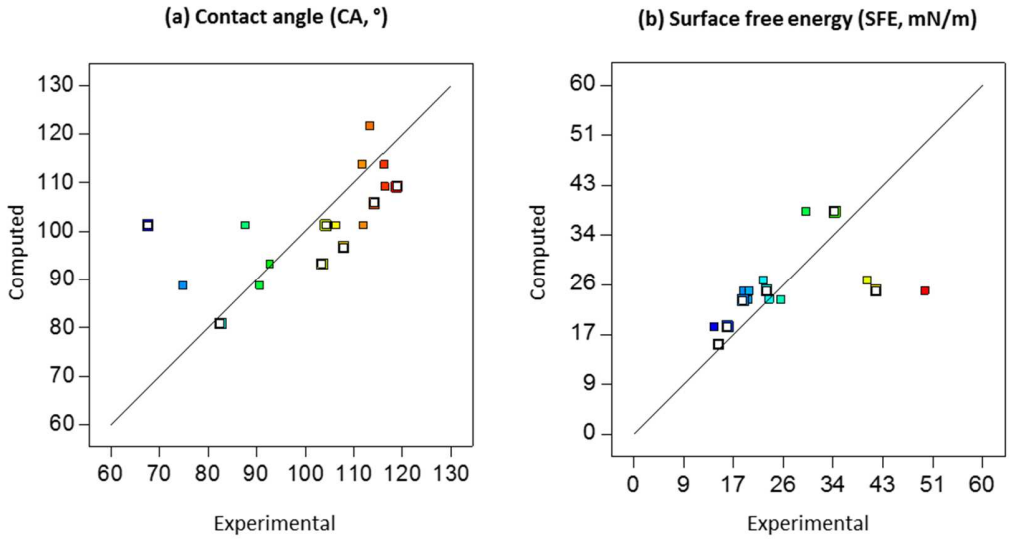

Figure 5: Computed value vs experimental data for (a) contact angle and (b) surface free energy

Concerning LEP, it varied between 1.5 – 2.05 bar during Runs 1- 17 even though the operating conditions varied significantly (**Figure 6(e)).** It can be observed w.r.t the standard deviation that the LEP_w fluctuated between 0.06- 0.5 bars within all the samples but did not deviate as compared to LEP_{ref} 2.05 bar. Based on ANOVA tests under the studied conditions, no correlation could be established between LEP and the operating conditions. In the present study, the only

information that could be deduced was that a decrease in LEP was observed after each experimental run compared with the LEP_{ref}.

As for CA, the computed values are higher than the experimental ones for the lowest values (below 80°), but the accuracy is good above this limit value. Similarly, accuracy is good for SFE for most data with three exceptions at the higher end as seen in **Figure 5(b)**. The calculated values obtained for CA and SFE and the experimental values of LEP_w are presented in **Figure 6.**

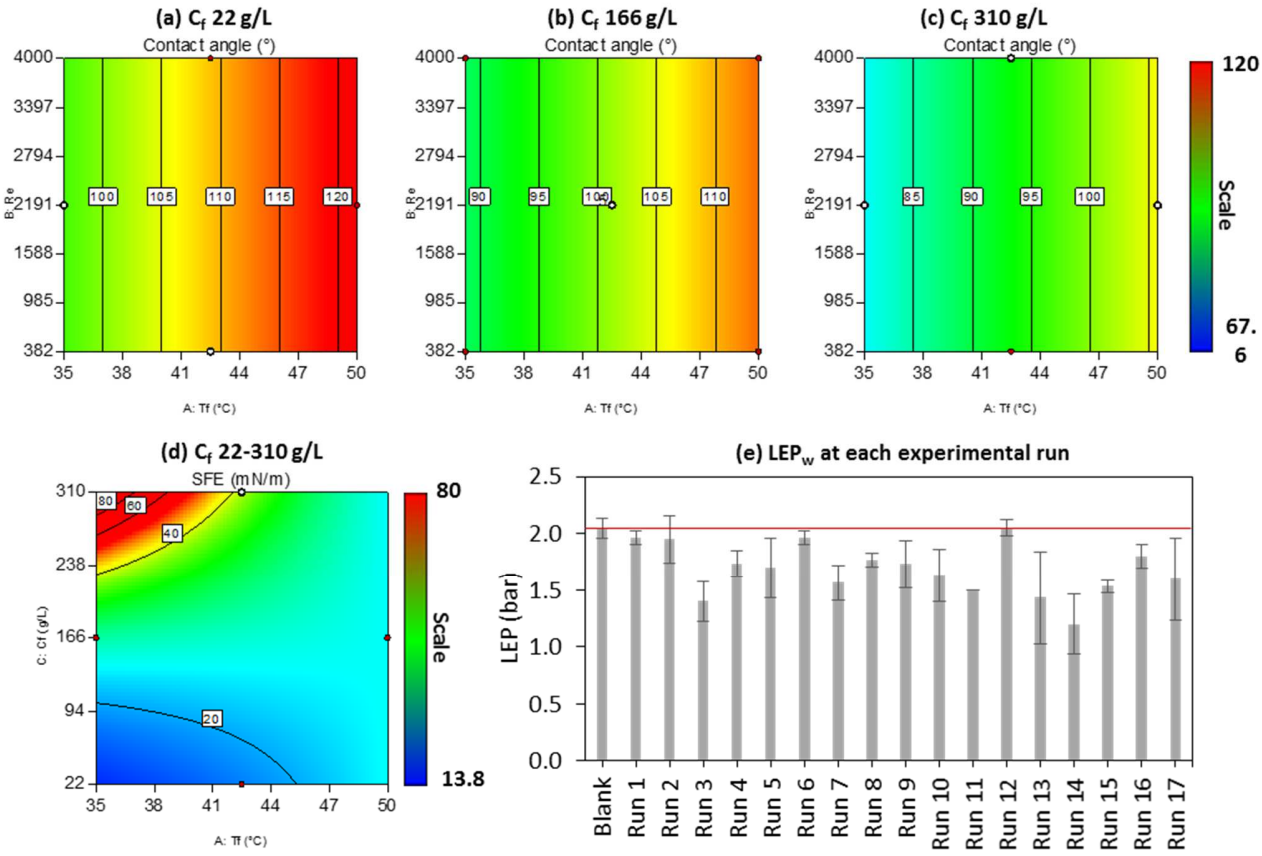

Figure 6: Calculated values at (a) 22 g/L (b) 166 g/L and (c) 310 g/L NaCl concentrations for Contact angle (d) SFE at 22-310 g/L NaCl and (e) experimental values of LEP for the 17 runs (to be viewed in color)

Figure 6 shows clearly that whatever the concentration, CA is not influenced by Re (which is not a parameter in Eq. 6) but is influenced by T_f. For each concentration (see Figure 6 **a, b and c**), CA

increases with an increase in temperature, and it is close to the CA of the virgin membrane at the higher temperature (50°C). These results on the influence of temperature are in contradiction with the observations [17] reporting a reduction in contact angle with an increase in temperature for samples tested with 35 g/L NaCl solutions. For the lower C_f value(22 g/L), the contact angle computed by Eq. 6 (Figure 6 (a, b, c)) is always lower than the one of the virgin membrane, and thus a loss of hydrophobicity occurs, and the lowest obtained value was 67.6°. This is consistent with literature reporting significant variation in CA even at low saline concentrations. For example, loss in membrane hydrophobicity was observed after 1 [35] to 30 h [36] of operation with seawater in DCMD configuration. When salinity increases from 22 g/L Figure 6 (a) to 166 g/L Figure 6 (b) and 310 g/L Figure 6 (c), the value of CA obtained at the lower temperature (35°C) decreases, meaning that the membrane becomes less hydrophobic. At this temperature, for 166 g/L the CA was about90°, and corresponds to the limit of hydrophobicity. For 310 g/L the CA was 81°, which corresponds to hydrophilicity.

The lower the surface free energy, the higher is the membrane hydrophobicity with lesser tendency to interact with the feed solution. **Figure 8 (d)** shows that SFE is close to the one of the virgin membrane (11.55+ 3.8 mN/m) for low temperatures and low concentrations. Its value increases when concentration increases and its maximal value (50.1 mN/m) is observed at the highest concentration and lower temperature. It is noticeable that this set of operating conditions also corresponds to the highest value of ω_s, and thus high SFE are correlated with a high proportion of total wetting.

3.2 Part 2: Influence of operating parameters on partial pore wetting

In the second part of the study, in order to better understand the influence of salt concentration at the early stage of wetting, that is to say during liquid intrusion in pores, independent experiments were performed at varying saline concentrations C_f with identical other operating conditions (cf.**2.2**). Both pore wetting, and wettability were assessed using the pore wetting ratio ω_p and the 3 wettability indicators: CA, SFE and, LEP_w.

3.2.1 Influence of salinity on pore wetting ratio (ω_p)

All the studied membranes were sampled at the same locations to reduce bias based on sampling locations. Pore wetting ratio for each location on the studied membrane are summarized in **Table 4** and the Cl^- intensity profiles (for B1-D2) are presented in **Figure 7.**

Based on the ω_p evaluation, for a salinity of 22 g/L, no wetting was observed for 5 samples, whereas surface, partial and total wetting were observed at 3, 1 and 1 locations respectively. As the salinity increases, the number of no wetting observations (w_p = 0) could be seen to be diminishing. As seen in **Table 4**, for all salinities at least 1 sample was observed to have total wetting, and the worst situation is observed for salinity of 250 g/L where total wetting (w_p = 100) had occurred at 6 sampling locations.

Table 4: Pore wetting ratio at each sampling location on the membrane surface

Salinity	Pore wetting ratio (ω_p)									
(g/L)	A1	A2	B1	B2	C1	C2	D1	D2	E1	E2
22	2.2	0	3.5	3.5	0	0	0	64.5	0	99.2
35	3.4	2.2	100	1.6	0	0	2.5	2.4	0	0
60	100	0	99.7	1.6	100	1.8	2.3	10.9	1.5	2.3
100	0	1.2	30.8	100	2.3	84.8	1.7	0.6	0	98.1
130	0	0	78.6	56.8	60.3	4.4	2.8	0	100	2
166	2.4	2.3	97.1	2.1	11.3	1.3	2.7	0	2.4	0.3
200	100	2.8	0.8	1.9	0.6	0	0.6	1.3	2.4	1.7
250	0.6	1.7	100	100	100	100	100	100	2	0
310	2.2	87.9	2.1	2.6	2.5	10.1	2.5	100	0.9	100

The variation in w_p is an indication of motion of the L/V interface at the local scale. To reveal more information about the influence of salinity on wetting mechanisms, analysis of different wetting mechanisms can be made by comparing the different gray value profiles obtained for the membranes subjected to different salinities. As nine saline solutions were studied they were categorized into 3 broad groups considering the salinity of the solution as follows:

1. Low to medium salinity (22, 35, 60 g/L NaCl solutions): **Figure 7** (a,b,c)

2. Medium to high salinity (100, 130, 166 g/L NaCl solutions): **Figure 7** (d,e,f)
3. High to hyper-salinity (200, 250, 310 g/L NaCl solutions): **Figure 7** (g,h,i)

In each figure, the x-axis is the membrane cross-section while the y-axis is the Cl^- intensity profile through the membrane cross-section at sampling locations (B1-D2) which are in the more central part of the filtration cell, where the flow is well established. At low to medium salinity, a progressive increase in surface wetting can be observed. As the salinity increases from 22 to 60 g/L NaCl, more and more sampling locations present surface wetting. Whereas, partial wetting was only detected at C_f 22 g/L and total wetting was observed at both 35 and 60 g/L NaCl concentrations.

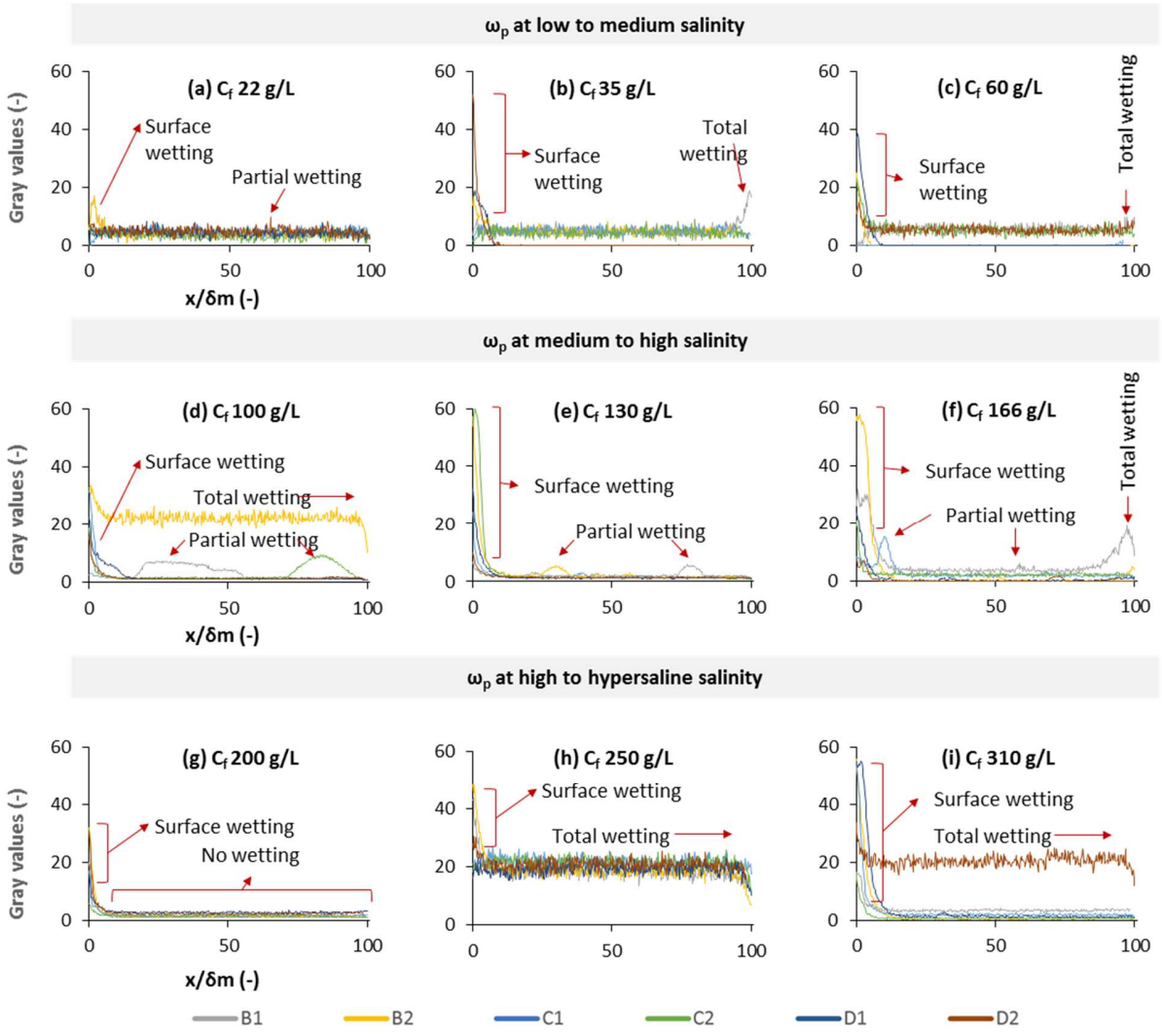

Figure 7: Sampling membrane cross-section for Cl^- intensity at (a,b,c) low to medium salt concentrations (d,e,f) medium to high salt concentrations (g,h,i) high to hypersaline salt concentrations (to be viewed in color)

Observations at medium to high feed salt concentration (100-166g/L), show that surface wetting started to become dominant with an increase in observations as compared to no wetting for this range of salinity. In **Figure 7** (d,e & f), various Cl^- peak intensities at different sampling locations can be observed indicative of partial wetting. Some of these observations are labeled on the **Figure** for easier visualization. These observations are attributed to a slight motion of L/V interface inside pores. Also, it must be noted that some cases (or locations) of partial wetting and total wetting are also observed in this group (for example in locations E1 and B1).

At high to hypersaline concentration (200- 310g/L NaCl), the behavior is very different at 200 g/L and at higher concentrations. Only surface wetting or no wetting was observed at 200 g/L NaCl solution in the central parts of the cell (locations B1-D2). At C_f 250 and 310 g/L surface wetting was also observed.

Moreover, for most locations at 250 g/L and one location at 310 g/L the profile corresponds to a uniform high intensity of Cl^- across all the membrane cross-section. This is the proof of intrusion of liquid along all the membrane thickness that is to say of total pore wetting, occurring at the local scale. It means that the L/V interface has been disrupted, leading to the convective transportation of the feed through the membrane pores. It can be deduced that greater interactions between the feed solution due to salinity, and maybe to crystallization due to saturation at the membrane surface could lead to frequent wetting occurrences. However, at this stage the link between crystallization and wetting (according to our definition) is not established. Literature complements the evidence of an increase in wettability at higher salt concentrations [37,38] and some researchers have suggested to use thickener membrane for higher salinities [20]. A general trend emerges that the frequency of surface, partial and total wetting increases from low salinity to hypersaline concentrations and that, for the studied

membrane, the occurrence of total wetting becomes significant for the more hypersaline solutions.

3.2.2 Influence of partial pressure and saline solution on sampling location for wetting

Due to the observations of various wetting mechanisms at all studied salinities, an effort was made to visualize the effects of the partial pressure of the saline solution (**Figure 8**(a)) at one location and salinity (**Figure 8**(b)) concerning all sampling locations. **Figure 8**(a)) presents the averaged value of pore wetting ratio at locations C1 and C2 as a function ΔP_{H20} (using Eq. 8)

$$\Delta P_{H20} = P_m - P_p = \alpha_{H20}.P_m^* - P_p \qquad \text{Eq. 8}$$

Where, ΔP_{H20} is the difference in partial pressure on both sides of the membrane (kPa), α_{H20} is the activity coefficient of water calculated at 42.5°C using PHREEQC-2, χ_{NaCl} molar fraction of water with NaCl in the feed solution and P_m^* is the partial pressure (kPa) of pure water at 42.5°C and P_p is the partial pressure of water on the permeate side.(kPa)

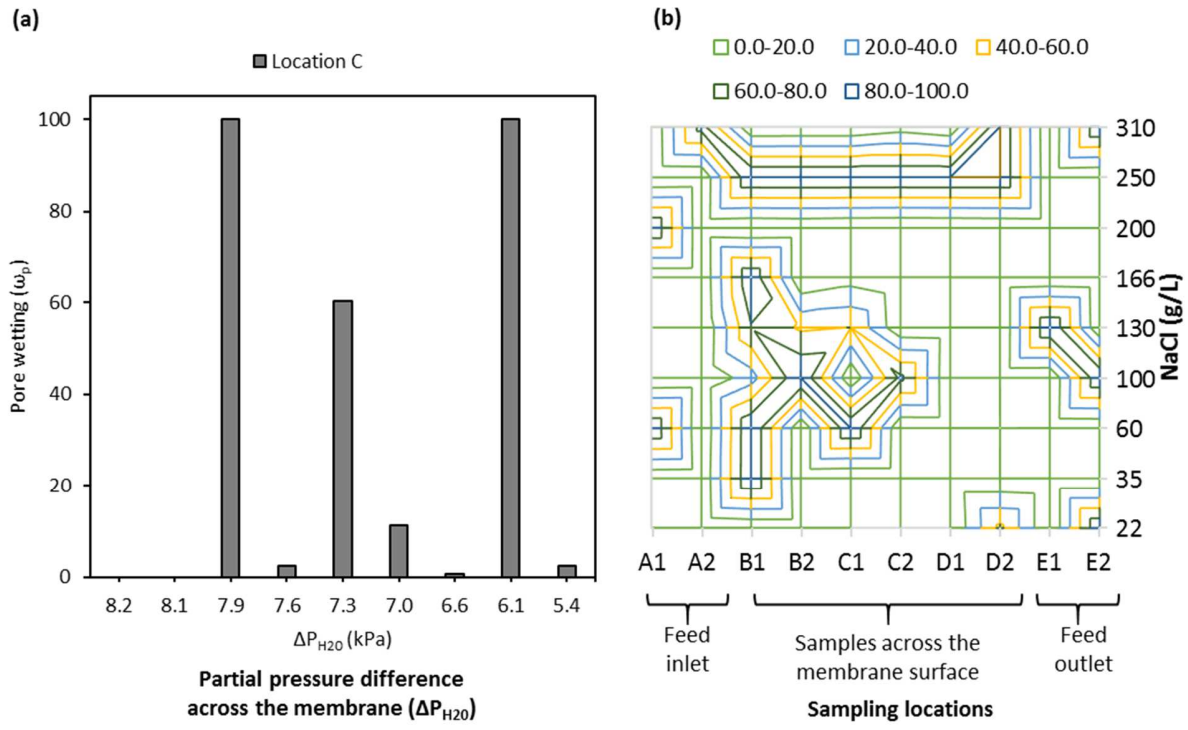

Figure 8: Location based pore wetting (ω_p) (a) at location C for different ΔP_{H20} (b) at all sampling locations at different NaCl concentrations (to be viewed in color)

In **Figure 8**(a)) it can be observed that at a given location (C) under the same operating conditions (T_f 42.5°C and Re 2191) there is no relationship between w_p and partial pressure. However, it can be noted that at the higher partial pressure of 8.2 and 8.1 kPa (that is to say C_f 22 and 35 g/L) no pore wetting was observed. By taking into account the partial pressure difference (ΔP_{H20}) experienced by the membrane, pore wetting ratio (ω_p) at this location (C) fluctuates to varying intensities. One possible explanation for this random comportment is that w_p is measured at the local scale and that the heterogeneity of membrane morphology at the local scale (surface charge, roughness and pore size distribution) might be responsible for these large variations.

On the other hand, **Figure 8** (b) presents ω_p as a 2D plot, where the sampling location from A1 to E2 are represented on the x-axis, while the y-axis presents all the studied salinities. A color code was defined, where ω_p is categorized by groups of 20 depending on the intensity, where 0-20 being no to little pore wetting and 80-100 being total pore wetting. Based on this figure, it can be inferred that most wetting occurrences on the membrane surface were observed near to the feed inlet (Sampling locations A1-C1) and some across the membrane surface with few observations on the feed outlet. This is indicative of the influence of pressure drop on wetting as the feed flows from the module's inlet to the outlet. However, several occurrences of various wetting mechanisms can be observed at high to hypersaline solution at C_f 200 to 310 /L.

The membrane cell used in this study is designed like conventional flat sheet cell, and similar to commercially available MD filtration cells for laboratories where the inlet and outlet ports of the membrane module are located directly under the membrane surface at each end. This creates a high-pressure zone at the inlet, some low-pressure zones at the outlet and some dead zones on the edge of the membrane. This high pressure drop on the membrane surface may be more favorable to induce wetting as demonstrated by more wetting observations close to the feed inlet port. So, in order to avoid wetting a specific attention should be paid to module design to

limit the risk of wetting in these specific areas. The DDTI method could be an interesting tool to help orientate the design, by testing different configurations.

3.2.3 Influence of salinity on wettability indicators

Wettability indicators present similar trends as the first part of this study. **Figure 9** shows clearly that CA and SFE have a linearity with salinity. Where CA is a linear decreasing function of the salt concentration and surface free energy is also linearly increasing as a function of the concentration which could be attributed to a negative interaction of increasing salinity on this membrane surface after operation. The increase in salinity globally implies loss of membrane's hydrophobicity as compared to CA_{ref} and SFE_{ref}. The fluctuation in standard deviation within each sample varied greatly for both CA and SFE, indicating the heterogeneity of interactions on the membrane surface.

With respect to liquid entry pressure here again, as in the first part of this study, this parameter appears as very constant and without sensitivity to salinity. The only definitive interpretation could be that LEP fluctuated with a slight decrease from the membrane's virgin properties.

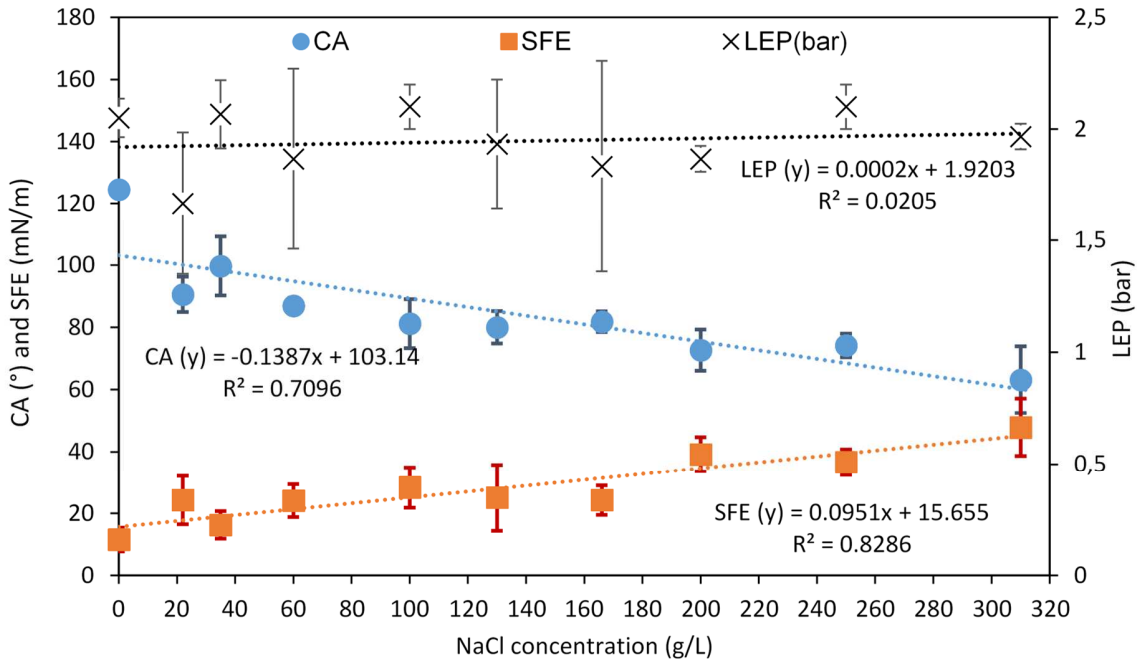

Figure 9: Relationship between saline concentration and wettability parameters (a) CA (b) SFE on the primary y-axis and (c) LEP on the secondary y-axis

However, it's interesting to note after washing the membrane surface with D.I. water there was a significant restoration of the membrane wettability indicators (CA and SFE) as compared to CA_{ref} and SFE_{ref}. As seen in **Figure 10 (a and b)** after washing, contact angle was restored to 90° but to varying degrees and linearity could not be established. Comparatively, the SFE after washing did reduce but fluctuated greatly both within the same sample and across salinities. No linear trends could be observed for the cleaned membranes for both wettability indicators. This rather reveals the discrepancy in interactions on the membrane surface even after cleaning.

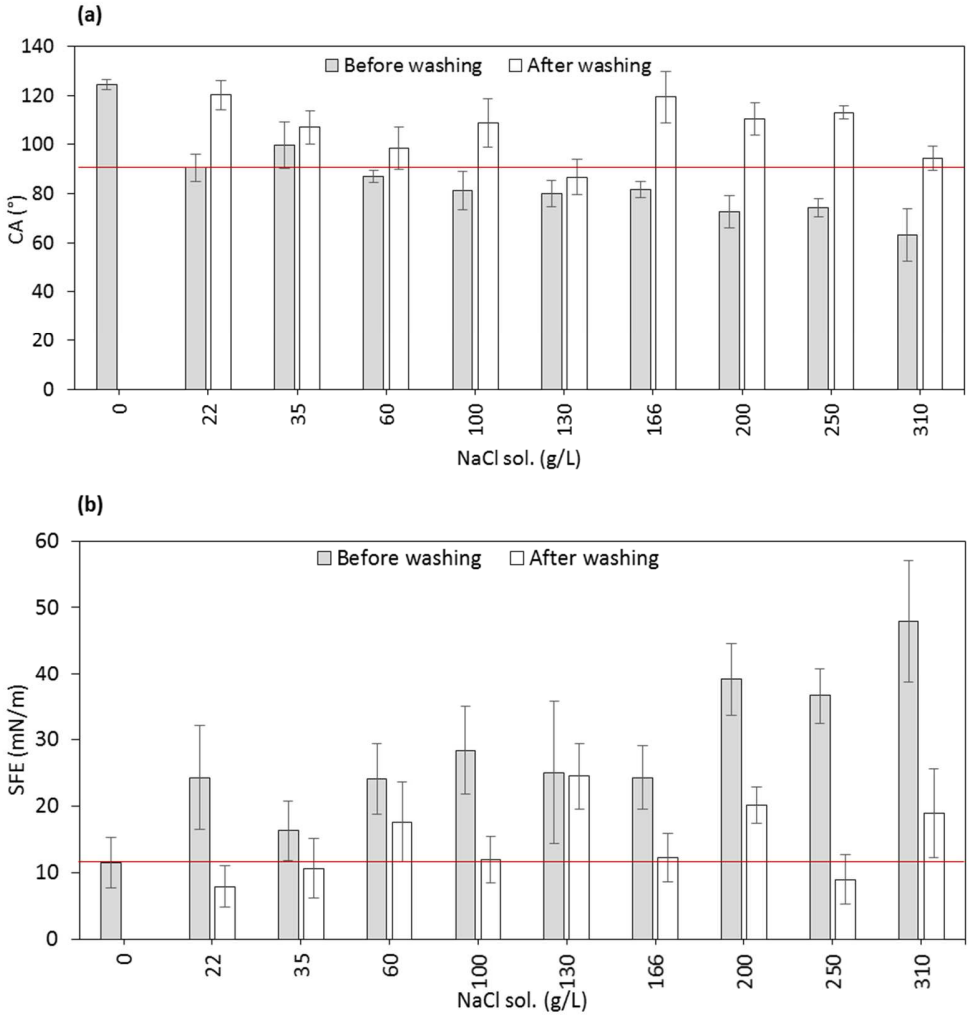

Figure 10*:* Wettability indicators (a) contact angle (b) surface free energy before and after cleaning the membrane surface

Further research and interpretation are needed on SFE as contributions towards polar and disperse interaction on the membrane surface were not the same as in virgin membrane. As PVDF material has only disperse component and after being subjected to the operating conditions with increasing solute concentrations there was a significant increase in polar interactions. Even though it may seem like the overall SFE had reduced but the surface properties were modified. However, the evaluation of the capability to restore the non-wetting properties of a wetted membrane is still to be performed.

4 Conclusions and perspectives

The growing interest in commercializing membrane distillation necessitates a deeper understanding to choose better membranes and operating parameters to prevent the risk of wetting. This study aimed at understanding the potential interactions of temperature (35 – 50°C), Reynolds number (400 – 4000) and salinity (22 – 310 g/L NaCl solution) on wetting during VMD operation with a PVDF membrane (0.22 µm). Wetting was evaluated using the recently developed DDTI method together with wettability indicators (LEP, CA and SFE).

In the first part of the study the interactions between the operating parameters on total wetting were studied using a Box Behnken design of experiments. The generated model did reveal some complex interactions between the three operating parameters on totally wetted surface ratio (wetting indicator) and wettability indicators (CA and SFE) with salinity (C_f) being a more sensitive parameter. At feed salinities lower than 166 g/L NaCl, totally wetted surface ratio (ω_s) was marginally affected by a change in temperature and Reynolds number. However, at hypersaline concentrations (C_f 310 g/L), an increase in temperature and Reynolds number facilitated avoiding total wetting. CA and SFE are the intrinsic membrane properties which were only affected by the temperature and salinity, but no interactions were identifiable considering Reynolds number. Though care should be taken as the models do diverge at the extremities of the design space resulting in discrepancies in computes and experimental values.

In the second step of the study, the feed temperature (42.5°C) and Reynolds numbers (2199) were fixed while the feed salinity was varied to quantify liquid intrusion in the PDVF membrane pores using the pore wetting ratio (ω_p). It appears that an increase in salinity primarily induces surface wetting which later results in either partial or total wetting with an evidence of total wetting only for hypersaline concentrations (higher than 200 g/L). However, it is clear that CA and SFE vary linearly with salinity as membrane hydrophobicity decreases and surface interactions increase with an increase in salinity. However, LEP is not significantly affected by salinity and remains almost constant

As a conclusion, this study showed that the operating parameters must be chosen carefully to prevent wetting and that for hypersaline solutions the choice of the membrane itself is a key issue. Future studies could continue using the DDTI method to further determine the conditions for making membrane distillation even more reliable. Focus could be given on the influence of vacuum pressures and on membrane screening in order to select some membranes that are less sensitive to hypersaline solutions. Additionally, special attention should be paid in designing membrane distillation modules to reduce the impact of wetting occurrences due to local hydrostatic pressure.

References

[1] TechNavio, Global Desalination Market 2018-2022, Research and Markets, Dublin, Ireland, 2018. https://www.researchandmarkets.com/research/tbss7g/global?w=4 (accessed June 21, 2018).

[2] A. Deshmukh, C. Boo, V. Karanikola, S. Lin, A.P. Straub, T. Tong, D.M. Warsinger, M. Elimelech, Membrane Distillation at the Water-Energy Nexus: Limits, Opportunities, and Challenges, Energy Environ. Sci. (2018).

[3] J.-P. Mericq, S. Laborie, C. Cabassud, Vacuum membrane distillation for an integrated seawater desalination process, Desalination Water Treat. 9 (2009) 287–296.

[4] J.-P. Mericq, S. Laborie, C. Cabassud, Evaluation of systems coupling vacuum membrane distillation and solar energy for seawater desalination, Chem. Eng. J. 166 (2011) 596–606. doi:10.1016/j.cej.2010.11.030.

[5] M.S. El-Bourawi, Z. Ding, R. Ma, M. Khayet, A framework for better understanding membrane distillation separation process, J. Membr. Sci. 285 (2006) 4–29. doi:10.1016/j.memsci.2006.08.002.

[6] M. Khayet, Membranes and theoretical modeling of membrane distillation: A review, Membr. Sep. Colloid Sci. 164 (2011) 56–88. doi:10.1016/j.cis.2010.09.005.

[7] M. Gryta, Fouling in direct contact membrane distillation process, J. Membr. Sci. (2008). http://www.sciencedirect.com/science/article/pii/S0376738808007527.

[8] L.R. Fisher, P.D. Lark, An experimental study of the Washburn equation for liquid flow in very fine capillaries, J. Colloid Interface Sci. 69 (1979) 486–492.

[9] E.W. Washburn, The dynamics of capillary flow, Phys. Rev. 17 (1921) 273.

[10] A.C.M. Franken, J.A.M. Nolten, M.H.V. Mulder, D. Bargeman, C.A. Smolders, Wetting criteria for the applicability of membrane distillation, J. Membr. Sci. 33 (1987) 315–328. doi:http://dx.doi.org/10.1016/S0376-7388(00)80288-4.

[11] B.S. Kim, P. Harriott, Critical entry pressure for liquids in hydrophobic membranes, J. Colloid Interface Sci. (1987). http://www.sciencedirect.com/science/article/pii/0021979787900026.

[12] P. Yazgan-Birgi, M.I. Hassan Ali, H.A. Arafat, Estimation of liquid entry pressure in hydrophobic membranes using CFD tools, J. Membr. Sci. 552 (2018) 68–76. doi:10.1016/j.memsci.2018.01.061.

[13] M.R. Qtaishat, T. Matsuura, 13 - Modelling of pore wetting in membrane distillation compared with pervaporation A2 - Basile, Angelo, in: A.F. Khayet (Ed.), Pervaporation Vap. Permeat. Membr. Distill., Woodhead Publishing, Oxford, 2015: pp. 385–413. http://www.sciencedirect.com/science/article/pii/B9781782422464000131.

[14] P. Jacob, S. Laborie, C. Cabassud, Visualizing and evaluating wetting in membrane distillation: New methodology and indicators based on Detection of Dissolved Tracer Intrusion (DDTI), Desalination. 443 (2018) 307–322. doi:10.1016/j.desal.2018.06.006.

[15] Y. Chen, Z. Wang, G.K. Jennings, S. Lin, Probing Pore Wetting in Membrane Distillation Using Impedance: Early Detection and Mechanism of Surfactant-Induced Wetting, Environ. Sci. Technol. Lett. (2017). doi:10.1021/acs.estlett.7b00372.

[16] M. Gryta, The influence of the hydrodynamic conditions on the performance of membrane distillation, in: Hydrodyn.-Optim. Methods Tools, InTech, 2011.

[17] R.B. Saffarini, B. Mansoor, R. Thomas, H.A. Arafat, Effect of temperature-dependent microstructure evolution on pore wetting in PTFE membranes under membrane distillation conditions, J. Membr. Sci. 429 (2013) 282–294. doi:10.1016/j.memsci.2012.11.049.

[18] M. Gryta, Degradation of Polypropylene Membranes Applied in Membrane Distillation Crystallizer, Crystals. 6 (2016) 33.

[19] E. Guillen-Burrieza, M.O. Mavukkandy, M.R. Bilad, H.A. Arafat, Understanding wetting phenomena in membrane distillation and how operational parameters can affect it, J. Membr. Sci. 515 (2016) 163–174. doi:10.1016/j.memsci.2016.05.051.

[20] L. Eykens, I. Hitsov, K. De Sitter, C. Dotremont, L. Pinoy, I. Nopens, B. Van der Bruggen, Influence of membrane thickness and process conditions on direct contact membrane distillation at different salinities, J. Membr. Sci. 498 (2016) 353–364. doi:10.1016/j.memsci.2015.07.037.

[21] L. Han, Y.Z. Tan, T. Netke, A.G. Fane, J.W. Chew, Understanding oily wastewater treatment via membrane distillation, J. Membr. Sci. 539 (2017) 284–294. doi:10.1016/j.memsci.2017.06.012.

[22] S. Velioğlu, L. Han, J.W. Chew, Understanding membrane pore-wetting in the membrane distillation of oil emulsions via molecular dynamics simulations, J. Membr. Sci. 551 (2018) 76–84.

[23] G.E.P. Box, D.W. Behnken, Simplex-Sum Designs: A Class of Second Order Rotatable Designs Derivable From Those of First Order, Ann Math Stat. (1960) 838–864. doi:10.1214/aoms/1177705661.

[24] M. Khayet, C. Cojocaru, C. García-Payo, Application of Response Surface Methodology and Experimental Design in Direct Contact Membrane Distillation, Ind. Eng. Chem. Res. 46 (2007) 5673–5685. doi:10.1021/ie070446p.

[25] P. Onsekizoglu, K. Savas Bahceci, J. Acar, The use of factorial design for modeling membrane distillation, J. Membr. Sci. 349 (2010) 225–230. doi:10.1016/j.memsci.2009.11.049.

[26] M. Khayet, C. Cojocaru, A. Baroudi, Modeling and optimization of sweeping gas membrane distillation, Spec. Issue Honour Profr. Takeshi Matsuura His 75th Birthd. 287 (2012) 159–166. doi:10.1016/j.desal.2011.04.070.

[27] M. Khayet, C. Cojocaru, Air gap membrane distillation: Desalination, modeling and optimization, Spec. Issue Honour Profr. Takeshi Matsuura His 75th Birthd. 287 (2012) 138–145. doi:10.1016/j.desal.2011.09.017.

[28] T.D. Dao, S. Laborie, C. Cabassud, Direct As(III) removal from brackish groundwater by vacuum membrane distillation: Effect of organic matter and salts on membrane fouling, Sep. Purif. Technol. 157 (2016) 35–44. doi:10.1016/j.seppur.2015.11.018.

[29] Y.Z. Tan, L. Han, W.H. Chow, A.G. Fane, J.W. Chew, Influence of module orientation and geometry in the membrane distillation of oily seawater, Desalination. 423 (2017) 111–123. doi:10.1016/j.desal.2017.09.019.

[30] M. Monnot, S. Laborie, C. Cabassud, Granular activated carbon filtration plus ultrafiltration as a pretreatment to seawater desalination lines: Impact on water quality and UF fouling, Desalination. 383 (2016) 1–11. doi:10.1016/j.desal.2015.12.010.

[31] W.M. Haynes, CRC Handbook of Chemistry and Physics, CRC press, 2014.

[32] J. Drelich, Guidelines to measurements of reproducible contact angles using a sessile-drop technique, Surf. Innov. 1 (2013) 248–254.

[33] A. Marmur, C. Della Volpe, S. Siboni, A. Amirfazli, J.W. Drelich, Contact angles and wettability: Towards common and accurate terminology, Surf. Innov. 5 (2017) 3–8.

[34] J. Zolgharnein, A. Shahmoradi, J.B. Ghasemi, Comparative study of Box–Behnken, central composite, and Doehlert matrix for multivariate optimization of Pb (II) adsorption onto Robinia tree leaves, J. Chemom. 27 (2013) 12–20.

[35] B. Zhang, L. Liu, S. Xie, F. Shen, H. Yan, H. Wu, Y. Wan, M. Yu, H. Ma, L. Li, J. Li, Built-up superhydrophobic composite membrane with carbon nanotubes for water desalination, RSC Adv. 4 (2014) 16561–16566. doi:10.1039/C3RA47436D.

[36] L.D. Nghiem, F. Hildinger, F.I. Hai, T. Cath, Treatment of saline aqueous solutions using direct contact membrane distillation, Desalination Water Treat. 32 (2011) 234–241.

[37] M. Gryta, Direct contact membrane distillation with crystallization applied to NaCl solutions, Chem. Pap.-SLOVAK Acad. Sci. 56 (2002) 14–19.

[38] M. Gryta, Concentration of NaCl solution by membrane distillation integrated with crystallization, Sep. Sci. Technol. 37 (2002) 3535–3558. doi:10.1081/SS-120014442.